On the Lasso for Graphical Continuous Lyapunov Models

Philipp Dettling* and Mathias Drton†

Technical University of Munich, Germany; TUM School of Computation, Information and Technology, Department of Mathematics and Munich Data Science Institute
e-mail: philipp.dettling@tum.de; mathias.drton@tum.de

Mladen Kolar

Booth School of Business
University of Chicago
e-mail: mladen.kolar@chicagobooth.edu

Abstract: Graphical continuous Lyapunov models offer a new perspective on modeling causally interpretable dependence structure in multivariate data by treating each independent observation as a one-time cross-sectional snapshot of a temporal process. Specifically, the models assume the observations to be cross-sections of independent multivariate Ornstein-Uhlenbeck processes in equilibrium. The Gaussian equilibrium exists under a stability assumption on the drift matrix, and the equilibrium covariance matrix is determined by the continuous Lyapunov equation. Each graphical continuous Lyapunov model assumes the drift matrix to be sparse with a support determined by a directed graph. A natural approach to model selection in this setting is to use an ℓ_1-regularization approach that seeks to find a sparse approximate solution to the Lyapunov equation when given a sample covariance matrix. We study the model selection properties of the resulting lasso technique by applying the primal-dual witness technique for support recovery. Our analysis uses special spectral properties of the Hessian of the considered loss function in order to arrive at a consistency result. While the lasso technique is able to recover useful structure, our results also demonstrate that the relevant irrepresentability condition may be violated in subtle ways, preventing perfect recovery even in seemingly favorable settings.

MSC2020 subject classifications: Primary 62H22, 62H12.
Keywords and phrases: Graphical models, irrepresentability, ℓ_1-regularization, Lyapunov equation, support recovery.

1. Introduction

1.1. Graphical Lyapunov Models

Graphical models are powerful tools for analyzing complex dependencies in multivariate observations. In particular, directed graphical models allow one to capture and explore dependencies induced by cause-effect relations (Pearl, 2009; Peters et al., 2017; Spirtes et al., 2000). The connection to causality is made by hypothesizing that each variable is a function of parent variables and independent noise. This approach is also known as structural causal modeling or structural equation modeling. For directed acyclic graphs (DAGs), the resulting models have simple interpretation and statistically favorable density factorization properties that facilitate large-scale analyses (Maathuis et al., 2019).

The situation is more complicated, however, when the graph is allowed to contain directed cycles, which represent feedback loops (Bongers et al., 2021). Although a statistical model can still be defined by solving the structural equations, directed cycles prevent density factorizations making it more difficult to solve tasks such as computation of maximum likelihood estimates (Drton et al., 2019) or model selection (e.g., Améndola et al., 2020; Richardson, 1996). Importantly, the interpretation of the models also becomes more involved and typically appeals to dynamic processes in a post-hoc way. For example, Fisher (1970) provided an interpretation based on data that are time averages. Alternative interpretations in terms of differential equations were suggested by Mooij et al. (2013) and Bongers and Mooij (2018).

Fitch (2019) and Varando and Richard Hansen (2020) proposed a different perspective, in which the starting point is a temporal process in equilibrium. That is, an i.i.d. sample $X_1, \ldots, X_n \in \mathbb{R}^p$ is assumed to arise from a multivariate Ornstein-Uhlenbeck process (i.e., a multivariate continuous-time autoregressive process) with X_i representing a single cross-sectional observation of the i-th process in equilibrium. Under this assumption, X_i is a multivariate normal random vector with a covariance matrix given by a (continuous) Lyapunov equation.

The p-dimensional Ornstein-Uhlenbeck process is the solution to the stochastic differential equation

$$\mathrm{d}X(t) = M(X(t) - a)\,\mathrm{d}t + D\,\mathrm{d}W(t), \tag{1}$$

where $W(t)$ is a Wiener process and $a \in \mathbb{R}^p$ and $M, D \in \mathbb{R}^{p \times p}$ are non-singular parameter matrices. The *drift matrix* M is the key object of interest in the work of Fitch (2019) and Varando and Richard Hansen (2020) as it determines the relations between the coordinates of the Ornstein-Uhlenbeck process $X(t)$; see also Mogensen et al. (2018). Provided M is stable (i.e., all eigenvalues have a strictly negative real part), $X(t)$ admits an equilibrium distribution that is multivariate normal with a positive definite covariance matrix. This covariance matrix, here denoted Σ, is determined as the unique matrix that solves the Lyapunov equation

$$M\Sigma + \Sigma M^\top + C = 0, \tag{2}$$

where $C = DD^\top$. The mean vector of the equilibrium distribution is a, the equilibrium state of the process. In the following, we will assume without loss of generality that our observations are centered, that is, $a = 0$. Moreover, we will focus on the case where the positive definite volatility matrix C is known up to a multiplicative scalar $\gamma > 0$. This accommodates, in particular, the homoscedastic case with $C = \gamma I_p$, where I_p denotes the identity matrix.

Our interest is now in the selection of models that postulate that the drift matrix $M = (M_{ij})$ is sparse. In other words, we consider the estimation of the sparsity pattern (or support) of the drift matrix M. This support is naturally represented by a directed graph $G = (V, E)$ with a vertex set $V = \{1, \ldots, p\}$ and an edge set E that includes the edge $i \to j$ precisely when $M_{ji} \neq 0$. A stable matrix M will have negative diagonal entries, and therefore the edge set E will always contain all self-loops $i \to i$. However, we will not draw the self-loops in figures showing graphs.

Example 1.1. The support of the matrix

$$M = \begin{pmatrix} m_{11} & 0 & 0 \\ m_{21} & m_{22} & 0 \\ 0 & m_{32} & m_{33} \end{pmatrix}$$

corresponds to the graph $G = (\{1, 2, 3\}, \{1 \to 2, 2 \to 3, 1 \to 1, 2 \to 2, 3 \to 3\})$, which is shown in Figure 1.

Fig 1: Directed graph on 3 nodes.

1.2. Identifiability

It is evident that the equilibrium distribution of the observations does not uniquely determine the pair of drift and volatility matrices (M, C). In particular, if (M, C) solves the Lyapunov equation, so does any scalar multiple of (M, C). Noting that scaling does not change the support of the drift matrix M, we see that to study the recovery of the support, we may assume without loss of generality that the volatility matrix C is fully known (the parameter γ may be scaled to be equal to one). This assumption is made throughout this paper.

Even after reducing to the case of a known volatility matrix C, the drift matrix M is not identifiable without exploiting further structure, such as sparsity. Indeed, the Lyapunov equation is a symmetric matrix equation with $(p+1)p/2$ individual equations, whereas M contains p^2 unknown parameters. However, M becomes identifiable when it is known to be suitably sparse. For example, it can be shown that the Lyapunov equation for a given C never has two different lower-triangular solutions. In particular, the matrix M from Example 1.1 can always be recovered uniquely from the Lyapunov equation when its graph/support is known. In a forthcoming companion paper (Dettling et al., 2022), we prove that unique recovery of M is always possible for graphs that do not contain cycles of length two. Many graphs with two-cycles permit almost sure unique recovery when the sparse entries of the drift matrix are selected randomly according to a continuous distribution, although here we cannot yet offer a concise sufficient condition.

1.3. Support Recovery with the Direct Lyapunov Lasso

In this paper, we will study an ℓ_1-regularization method for estimating the support of the drift matrix M from an i.i.d. sample consisting of centered observations $X_1, \ldots, X_n \in \mathbb{R}^p$. Let

$$\hat{\Sigma} = \hat{\Sigma}^{(n)} = \frac{1}{n} \sum_{i=1}^{n} X_i X_i^\top \tag{3}$$

be the sample covariance matrix. The *Direct Lyapunov Lasso* finds a sparse estimate of M as a solution of the convex optimization problem

$$\min_{M \in \mathbb{R}^{p \times p}} \frac{1}{2} \| M\hat{\Sigma} + \hat{\Sigma}M^\top + C \|_F^2 + \lambda \|M\|_1 \tag{4}$$

with the tuning parameter $\lambda > 0$. This method was considered in numerical experiments by Fitch (2019) as well as Varando and Richard Hansen (2020) who additionally explored non-convex methods based on regularizing Gaussian likelihood or a Frobenius loss for covariance matrix estimation.

Our main contribution is twofold. First, we derive a consistency result for support recovery using the primal-dual witness method. The Hessian in the quadratic part of the Direct Lyapunov Lasso objective does not concentrate well entry-wise and, thus, we modify the standard analysis to take advantage of spectral properties of the Hessian. Second, we study the irrepresentability condition that is assumed in the consistency result. We show that the condition may fail to hold
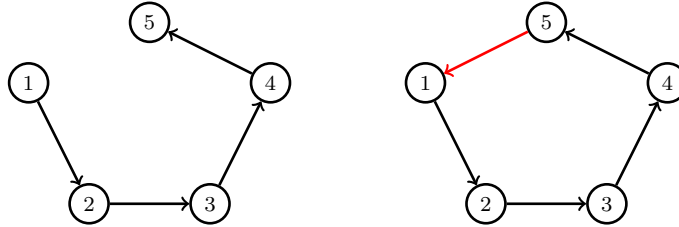
Fig 2: Left: The graph G_1, a path 1 to 5. Right: The graph G_2, the 5-cycle.

in seemingly favorable settings, particularly when the true support corresponds to a graph with directed cycles. Although the Direct Lyapunov Lasso may also recover useful structures in these settings, it is no longer able to perfectly recover the true support. We illustrate this point in the following example.

Example 1.2. Let G_1 be the path from 1 to 5, and let G_2 be the 5-cycle obtained by adding the edge $5 \to 1$; see Figure 2. For G_1 we define a (well-conditioned) stable matrix M_1^* by setting the diagonal to $(-2, -3, -4, -5, -6)$ and the four nonzero off-diagonal entries to 1. For G_2, we consider two cases. In the first case, we add the entry $m_{15} = 1$ to M_1^* to obtain the matrix M_2^*. We then draw 100 samples of size $n = 100, 200, 500, 1000, 5000, 10^4, 10^5, \infty$ from $N(0, \Sigma_j^*)$ for $j = 1, 2$, where Σ_j^* is the covariance matrix obtained from M_j^*. When $n = \infty$, the population covariance matrices are taken as input to the method. In the second case, we generate 100 stable matrices $M_{2,1}^*, \ldots, M_{2,100}^*$ from M_1^* by selecting 100 entries m_{15} according to a uniform distribution on $[0.5, 1.5]$. Let $\Sigma_{2,1}^*, \ldots, \Sigma_{2,100}^*$ be the corresponding equilibrium covariance matrices. In the second case, we generate one sample from $N(0, \Sigma_j^*)$, $j = 1, (2, 1), \ldots, (2, 100)$ for each of the sample sizes given above. Direct Lyapunov Lasso is used for support recovery, with the penalty parameter λ changing over a grid in $[10^{-1}, 10^{-7}]$. For each data set, we calculate the maximum accuracy (acc $= (tp + tn)/(tp + tn + fp + fn)$) over the regularization path, the maximum F_1-score (F_1-score $= tp/(tp + 1/2(fp + fn))$) over the regularization path, and the area under the ROC curve — the ROC curve displays $TPR = tp/(tp + fp)$ on the y axis and $FPR = fp/(tn + fp)$ on the x axis along the regularization path. These performance measures are based on the number of true positives (tp), true negatives (tn), false positives (fp), and false negatives (fn) that are computed by comparing the estimates with the true support.

The simulation results are shown in Figure 3. The blue curves show the scores for G_1 averaged over 100 independent samples, and the red and green curves display the scores for G_2. The red curves show the performance measures averaged over 100 independent samples for M_2^*, while the green curves show the performance measures averaged over 100 signals $M_{2,1}^*, \ldots, M_{2,100}^*$, with one sample signal available. We observe that for every sample size and performance measure, the Direct Lyapunov Lasso performs much better for the path G_1 then for the cycle G_2. When the sample size is $n = 10^5$, we observe a perfect recovery of G_1. However, increasing the sample size when recovering G_2 does not result in perfect recovery. Even when the population covariance matrix is used as the input to the Direct Lyapunov Lasso, the performance metrics do not improve over the case of $n = 10^5$. Also, the choice of $m_{15} = 1$ is not particularly unfortunate— averaging over various completions does not improve the metrics. We obtain useful estimates for both graphs, but it is evident that the path can be recovered perfectly for a sufficiently large sample size, while the cycle cannot be perfectly recovered. Our subsequent analysis explains this behavior, which is a consequence of the failure of the irrepresentability condition in (10).
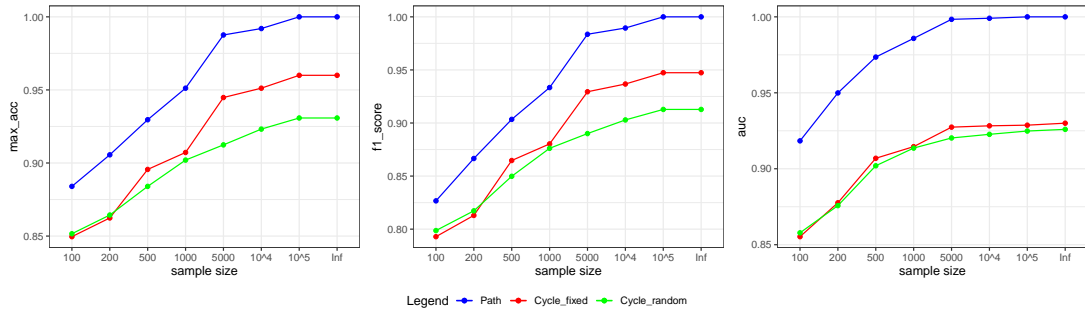
Fig 3: Performance measures for sample sizes $n = 10^1, \ldots, 10^6, \infty$ and models given by the graphs G_1 and G_2 from Figure 2, one choice of edgeweights for the path, 1000 random completions to the 5-cycle, Cycle-max is the maximal score across the 1000 completions and Cycle-mean is the average score. Left: maximal accuracy, Middle: maximal f_1-score, Right: area under the ROC curve.

1.4. Organization of the Paper

We first connect the Direct Lyapunov Lasso to more standard lasso problems by vectorizing the Lyapunov equation and describing the structure of the Hessian matrix for the smooth part of the Direct Lyapunov Lasso objective (Section 2). In Section 3, we derive a deterministic guarantee for support recovery based on the primal-dual witness approach (Theorem 3.1). We then extend this guarantee to a statistical consistency result (Corollary 3.2), where the solution $\hat{M}$ of (4) is shown to converge in the max norm at a rate $\|\hat{M} - M^*\|_\infty = O(\sqrt{(d \log p)/n})$ with d being the number of nonzero entries in the true drift matrix M^*. The necessary probabilistic analysis is based on the concentration results for the spectral norm of the sample covariance matrix, from which we are able to deduce the concentration results for the Direct Lyapunov Lasso Hessian (Section 4). Since some of the Hessian entries are quadratic polynomials involving p terms, this spectral point of view is key to our analysis as it yields sharper bounds than those one would be able to derive via the usual approach that considers entry-wise concentration for the analysis of lasso methods; see Lin et al. (2016) for one example of entry-wise analysis of a Hessian. Theorem 3.1 and Corollary 3.2 only hold under an irrepresentable condition, which turns out to be more subtle than in the classical lasso regression. As we explore in Section 5, the condition is highly dependent on the structure of the graph associated with the true signal and appears to be particularly restrictive for graphs with directed cycles. While for DAGs (directed acyclic graphs) we are able to always construct matrices at which the condition holds, a similar general construction for cyclic graphs seems more involved, and we can only point to small-scale examples generated from a larger number of simulations. We conclude the paper with a discussion in Section 6.

1.5. Notation

Let $b \in [1, \infty]$. The ℓ_b-norm of $v \in \mathbb{R}^p$ is $\|v\|_b = (\sum_{i=1}^p |v_i|^b)^{1/b}$, with $\|v\|_\infty = \max_{1 \leq i \leq n} |v_i|$. We may apply this vector norm to a matrix $A = (a_{ij}) \in \mathbb{R}^{p \times p}$ and obtain the norm $\|A\|_b = (\sum_{i=1}^p \sum_{j=1}^n |a_{ij}|^b)^{1/b}$. In particular, $\|A\|_F := \|A\|_2$ is the Frobenius norm. We denote the associated operator norm by $\|A\|_b = \max\{\|Ax\|_b : \|x\|_b = 1\}$. Specifically, we use $\|A\|_2$ to denote the spectral norm, given by the maximal singular value of A, and $\|A\|_\infty = \max_{1 \leq i \leq p} \sum_{j=1}^p |a_{ij}|$ to denote the maximum absolute row sum.

For an index set S, we write $A_{\cdot S}$ for the submatrix of A that is obtained by selecting the columns indexed by S. The matrices $A_{S\cdot}$ and A_{SS} are defined analogously by selection of rows or both rows and columns, respectively. The vec-operator turns the matrix $A = (a_{ij})$ into a vector in $\mathbb{R}^{p^2}$ by stacking its columns, so $\text{vec}(A) = (a_{11}, a_{21}, \ldots, a_{p1}, \ldots, a_{1p}, \ldots, a_{pp})^\top$. The diag-operator turns a vector $v \in \mathbb{R}^p$ into the diagonal matrix $\text{diag}(v) \in \mathbb{R}^{p \times p}$ that has v_i as its i-th diagonal entry. The Kronecker product of A and another matrix $B = (b_{uv}) \in \mathbb{R}^{p \times p}$ is denoted by $A \otimes B$. It is a matrix in $\mathbb{R}^{p^2 \times p^2}$ with the entries $[A \otimes B]_{(i-1)p+j,(k-1)p+l} = A_{ik}B_{jl}$. The commutation matrix in $\mathbb{R}^{p^2 \times p^2}$ is the permutation matrix $K^{(p,p)}$ that transforms the column vectorization of a matrix into its row vectorization, i.e., $K^{(p,p)}\text{vec}(A) = \text{vec}(A^\top)$. Let $e_{p,i}$ be the i-th canonical basis vector in $\mathbb{R}^p$. Then

$$K^{(p,p)} = \sum_{i=1}^{p}\sum_{j=1}^{p}(e_{p,i}e_{p,j}^\top) \otimes (e_{p,j}e_{p,i}^\top).$$

Put differently, the rows of $K^{(p,p)}$ are canonical basis vectors and $K^{(p,p)}_{(i-1)p+j,(j-1)p+i} = 1$ for $i, j = 1, \ldots, p$. See, e.g., Bernstein (2018) for further background.

Finally, we write Sym_p for the space of symmetric matrices in $\mathbb{R}^{p \times p}$. We use PD_p to denote the cone of $p \times p$ positive definite matrices. The set of stable matrices in $\mathbb{R}^{p \times p}$ is denoted Stab_p.

2. Gram Matrix of the Direct Lyapunov Lasso

In this section, we rewrite the smooth part of the objective of the Direct Lyapunov Lasso from (4) in terms of the vectorized drift matrix and present the resulting Hessian matrix.

The Lyapunov equation from (2) is a linear matrix equation and may be rewritten as

$$A(\Sigma)\,\text{vec}(M) + \text{vec}(C) = 0, \tag{5}$$

where the $p^2 \times p^2$ matrix $A(\Sigma)$ has its rows and columns indexed by pairs $(i,j) \in \{1, \ldots, p\}^2$ and takes the form

$$A(\Sigma) = (\Sigma \otimes I_p) + (I_p \otimes \Sigma)K^{(p,p)}. \tag{6}$$

We have $\text{vec}(M\Sigma) = (\Sigma \otimes I_p)\text{vec}(M)$ and $\text{vec}(\Sigma M^\top) = (I_p \otimes \Sigma)K^{(p,p)}\text{vec}(M)$. By the symmetry of the Lyapunov equation, $A(\Sigma)$ has two copies of each row corresponding to an off-diagonal entry in the Lyapunov equation. Retaining this redundancy will be helpful for later arguments, as it preserves the Kronecker product structure in (6).

Example 2.1. When $p = 3$, the matrix $A(\Sigma)$ is a 9×9 matrix and has the form

	$(1,1)$	$(1,2)$	$(1,3)$	$(2,1)$	$(2,2)$	$(2,3)$	$(3,1)$	$(3,2)$	$(3,3)$
$(1,1)$	$2\Sigma_{11}$	0	0	$2\Sigma_{12}$	0	0	$2\Sigma_{13}$	0	0
$(1,2)$	Σ_{21}	Σ_{11}	0	Σ_{22}	Σ_{12}	0	Σ_{23}	Σ_{13}	0
$(1,3)$	Σ_{31}	0	Σ_{11}	Σ_{23}	0	Σ_{12}	Σ_{33}	0	Σ_{13}
$(2,1)$	Σ_{21}	Σ_{11}	0	Σ_{22}	Σ_{12}	0	Σ_{23}	Σ_{13}	0
$(2,2)$	0	$2\Sigma_{21}$	0	0	$2\Sigma_{22}$	0	0	$2\Sigma_{23}$	0
$(2,3)$	0	Σ_{31}	Σ_{21}	0	Σ_{23}	Σ_{22}	0	Σ_{33}	Σ_{23}
$(3,1)$	Σ_{31}	0	Σ_{11}	Σ_{23}	0	Σ_{12}	Σ_{33}	0	Σ_{13}
$(3,2)$	0	Σ_{31}	Σ_{21}	0	Σ_{23}	Σ_{22}	0	Σ_{33}	Σ_{23}
$(3,3)$	0	0	$2\Sigma_{31}$	0	0	$2\Sigma_{23}$	0	0	$2\Sigma_{33}$

.

Rows with an italicized index correspond to strictly upper triangular entries in the Lyapunov equation from (2).

Define the *Gram matrix*

$$\Gamma(\Sigma) := A(\Sigma)^\top A(\Sigma) \ \in \mathbb{R}^{p^2 \times p^2} \tag{7}$$

and the vector

$$g(\Sigma) := -A(\Sigma)\text{vec}(C) \ \in \mathbb{R}^{p^2}. \tag{8}$$

Omitting a constant from the objective function, the Direct Lyapunov Lasso problem from (4) may be reformulated as

$$\min_{M \in \mathbb{R}^{p \times p}} \frac{1}{2} \text{vec}(M)^\top \Gamma(\hat{\Sigma})\text{vec}(M) - g(\hat{\Sigma})^\top \text{vec}(M) + \lambda \|\text{vec}(M)\|_1. \tag{9}$$

As noted in the introduction, one difficulty that arises in the analysis of the solution of (9) is the fact that the Gram matrix has entries that are quadratic polynomials in Σ with p terms (i.e., the number of terms scales with the size of the problem). This fact can be seen by the appearance of Σ^2 in the following formula for the Gram matrix.

Lemma 2.2. *The Gram matrix for a given covariance matrix Σ is equal to*

$$\Gamma(\Sigma) = A(\Sigma)^\top A(\Sigma) = 2(\Sigma^2 \otimes I_p) + (\Sigma \otimes \Sigma)K^{(p,p)} + K^{(p,p)}(\Sigma \otimes \Sigma).$$

Proof. Apply the rules $(A \otimes B)^\top = (A^\top \otimes B^\top)$, $(A \otimes B)(C \otimes D) = (AC) \otimes (BD)$ and $K^{(p,p)}(A \otimes B)K^{(p,p)} = B \otimes A$ to deduce that

$$
\begin{aligned}
A(\Sigma)^\top A(\Sigma) &= [(\Sigma \otimes I_p) + K^{(p,p)}(I_p \otimes \Sigma)][(\Sigma \otimes I_p) + (I_p \otimes \Sigma)K^{(p,p)}] \\
&= 2(\Sigma^2 \otimes I_p) + (\Sigma \otimes \Sigma)K^{(p,p)} + K^{(p,p)}(\Sigma \otimes \Sigma). \qquad \square
\end{aligned}
$$

3. Consistent Support Recovery with the Direct Lyapunov Lasso

In this section, we provide deterministic conditions under which the Direct Lyapunov Lasso is able to recover the support of the true population drift matrix that defines the data-generating distribution. Our conditions are obtained via Primal-Dual-Witness (PDW) method (Wainwright, 2009). Specifically, we adapt the PDW construction of Lin et al. (2016), who considered structure learning for undirected graphical models with score matching.

We start by introducing some more notation. The matrix M^* denotes the true drift matrix in (1) and $\hat{M}$ denotes the solution of the Direct Lyapunov Lasso problem in (4). The support of M^* is the set of all indices of nonzero elements and is denoted by

$$S \equiv S(M^*) = \{(j,k) : M^*_{jk} \neq 0\}.$$

We write $d = |S|$ for the size of the support of M^*. The support set of the estimate $\hat{M}$ is written

$$\hat{S} \equiv S(\hat{M}) = \{(j,k) : \hat{M}_{jk} \neq 0\}.$$

Let $\hat{\Gamma} = \Gamma(\hat{\Sigma})$, $\Gamma^* = \Gamma(\Sigma^*)$, $\hat{g} = g(\hat{\Sigma})$, $g^* = g(\Sigma^*)$. Furthermore, let $\Delta_\Gamma = \hat{\Gamma} - \Gamma^*$ and $\Delta_g = \hat{g} - g^*$, and define the quantities

$$c_{\Gamma^*} = \|(\Gamma^*_{SS})^{-1}\|_\infty \ \text{ and } \ c_{M^*} = \|\text{vec}(M^*)\|_\infty.$$

The definition of c_{Γ^*} requires Γ^*_{SS} to be invertible, which is an implicit assumption on the identifiability of the parameters; recall Section 1.2.

Theorem 3.1. *Let $M^* \in Stab_p$ be the true drift matrix, and let S be its support. Assume that Γ^*_{SS} is invertible and that the irrepresentable condition*

$$\|\Gamma^*_{S^c S}(\Gamma^*_{SS})^{-1}\text{sign}(\text{vec}(M^*))_S\|_\infty \le (1-\alpha) \tag{10}$$

holds with parameter $\alpha \in (0, 1]$. Furthermore, assume that $\hat{\Gamma}$ is a matrix such that

$$\|(\Delta_\Gamma)_{\cdot S}\|_\infty < \epsilon_1, \qquad \|\Delta_g\|_\infty < \epsilon_2,$$

with $\epsilon_1 \le \alpha/(6c_{\Gamma^*})$. Then if

$$\lambda > \frac{3(2-\alpha)}{\alpha}\max\{c_{M^*}\epsilon_1, \epsilon_2\},$$

then $\hat{M}$ is unique, has its support included in the true support $(\hat{S} \subseteq S)$, and satisfies

$$\|\hat{M} - M^*\|_\infty < \frac{c_{\Gamma^*}}{2-\alpha}\lambda.$$

In addition, if

$$\min_{\substack{1 \le j < k \le p \\ (j,k) \in S}} |M^*_{jk}| > \frac{c_{\Gamma^*}}{2-\alpha}\lambda,$$

then $\hat{S} = S$ and $\text{sign}(\hat{M}_{jk}) = \text{sign}(M^*_{jk})$ for all $(j,k) \in S$.

Proof. The proof is very similar to the proof of Theorem 1 in Lin et al. (2016), and we defer details to the Appendix A. $\qquad\square$

We note that the condition

$$\|\Gamma^*_{S^c S}(\Gamma^*_{SS})^{-1}\|_\infty < 1 - \alpha$$

is sufficient to prove Theorem 3.1. However, the formulation in (10) allows one to prove that irrepresentability is also an almost necessary condition, similar to Zhao and Yu (2006).

Theorem 3.1 provides a deterministic result for the estimation error and support recovery under a general bound on Δ_Γ and Δ_g. It leads to the following probabilistic result.

Corollary 3.2. *Suppose the data are generated as n i.i.d. draws from the Gaussian equilibrium distribution of a p-dimensional Ornstein-Uhlenbeck process defined by a drift matrix $M^* \in Stab_p$ and a matrix $C \in PD_p$. Let S be the support of M^*. Assume that Γ^*_{SS} is invertible and that the irrepresentability condition holds for $\alpha \in (0,1]$. Let*

$$c_{\Sigma^*} = \|\!|\Sigma^*|\!\|_2, \quad c_C = \|vec(C)\|_2, \quad \tilde{c} = \max\left\{\frac{(16 + 32c_{\Sigma^*})^2}{c_3}, \frac{16c_C^2}{c_3}, 16c_1^2\right\}, \quad c_* = \frac{6}{\alpha}c_{\Gamma^*},$$

where $\{c_i\}_{i=1}^3$ are universal constants (from Theorem 4.4 below) with $c_1 > 1$. Suppose the sample size satisfies $n > \tilde{c}d\log p^{\tau_1}\max\{c_*^2, 1/4\}$ for $\tau_1 \ge 2\log(c_2)/\log(p)$, and the regularization parameter is chosen as

$$\lambda > \frac{3c_{M^*}(2-\alpha)}{\alpha}\sqrt{\frac{\tilde{c}d\log p^{\tau_1}}{n}}.$$

Then the following statements hold with probability at least $1 - c_2 p^{-\tau_1}$:

a) *The minimizer $\hat{M}$ is unique, has its support included in the true support ($\hat{S} \subset S$), and satisfies*

$$\|\hat{M} - M^*\|_\infty < \frac{c_{\Gamma^*}}{2 - \alpha}\lambda.$$

b) *Furthermore, if*

$$\min_{\substack{1 \leq j < k \leq m \\ (j,k) \in S}} |M^*_{jk}| > \frac{c_{\Gamma^*}}{2 - \alpha}\lambda,$$

then $\hat{S} = S$ and $\mathrm{sign}(\hat{M}_{jk}) = \mathrm{sign}(M^*_{jk})$ for all $(j, k) \in S$.

The corollary follows from Theorem 3.1 together with the concentration results we obtain in Section 4. We defer the proof of Corollary 3.2 to the end of Section 4.

We emphasize that the crucial assumption for support recovery is the irrepresentability condition, which we investigate in detail in Section 5. In order for the Direct Lyapunov Lasso to succeed in support recovery, a sample size $n = \Omega(d \log p)$ is required; recall that $d = |S|$ is the size of the support of M^*. Since S includes the diagonal elements of M^*, we have that $d \geq p$. Under sparsity, however, d is much smaller than the number of unknown parameters p^2 making the consistency result high-dimensional.

To make a comparison to other (simpler) graphical models, we note that the sample size requirement of the graphical lasso is on the order of $d^2 \log p$ with d being the maximum number of nonzero entries in any row of a true precision matrix (Ravikumar et al., 2011). This allows for far higher-dimensional settings than our result above and is due to the glasso having a sample Hessian that concentrates well entry-wise and the simple connection between the covariance matrix and the sparse precision matrix. In contrast, our Lyapunov model has a more variable sample Hessian and a more complicated relationship between the covariance matrix and the sparse signal (i.e., drift matrix).

4. Probabilistic Analysis

As clarified in the previous section, success of the Direct Lyapunov Lasso depends on the loss being sufficiently close to its population version in the sense of $\Delta_\Gamma = \hat{\Gamma} - \Gamma^*$ and $\Delta_g = \hat{g} - g^*$ being sufficiently small. In this section, we bound Δ_Γ and Δ_g in terms of $\Delta_\Sigma = \hat{\Sigma} - \Sigma^*$ and, subsequently, use a concentration inequality for $\|\Delta_\Sigma\|_2$ to probabilistically bound Δ_Γ and Δ_g.

Deriving an inequality for $\hat{\Gamma}$ is most critical as the matrix contains sums of products of covariances and a careful analysis is required to obtain a non-trivial requirement on the sample size. Let $\Gamma(\Sigma) = \Gamma_1(\Sigma) + \Gamma_2(\Sigma)$, where

$$\Gamma_1(\Sigma) = 2(\Sigma^2 \otimes I_p) \quad \text{and} \quad \Gamma_2(\Sigma) = (\Sigma \otimes \Sigma)K^{(p,p)} + K^{(p,p)}(\Sigma \otimes \Sigma).$$

Lemma 4.1. *Let $c_{\Sigma^*} = \|\Sigma^*\|_2$. Then*

$$\|\Gamma_1(\hat{\Sigma}) - \Gamma_1(\Sigma^*)\|_2 \leq 2\|\Delta_\Sigma\|_2^2 + 4c_{\Sigma^*}\|\Delta_\Sigma\|_2.$$

Proof. Using that $\|A \otimes B\|_2 = \|A\|_2\|B\|_2$, we obtain that

$$\|\Gamma_1(\hat{\Sigma}) - \Gamma_1(\Sigma^*)\|_2 = 2\|(\hat{\Sigma}^2 - (\Sigma^*)^2) \otimes I_p)\|_2 = 2\|\hat{\Sigma}^2 - (\Sigma^*)^2)\|_2$$
$$\leq 2\|\Delta_\Sigma^2\|_2 + 2\|\Delta_\Sigma \Sigma^*\|_2 + 2\|\Sigma^* \Delta_\Sigma\|_2.$$

Since the spectral norm of a symmetric matrix is the absolute maximal eigenvalue, and the eigenvalues of a squared matrix are the squared eigenvalues of the original matrix, we find as claimed that

$$\|\Gamma_1(\hat{\Sigma}) - \Gamma_1(\Sigma^*)\|_2 \leq 2\|\Delta_\Sigma\|_2^2 + 4\|\Sigma^*\|_2\|\Delta_\Sigma\|_2. \qquad \square$$

Lemma 4.2. *Let $c_{\Sigma^*} = \|\Sigma^*\|_2$. Then*

$$\|\Gamma_2(\hat{\Sigma}) - \Gamma_2(\Sigma^*)\|_2 \leq 2\|\Delta_\Sigma\|_2^2 + 4c_{\Sigma^*}\|\Delta_\Sigma\|_2.$$

Proof. The commutation matrix $K^{(p,p)}$ is an orthonormal matrix. Therefore, $\|K^{(p,p)}\|_2 = 1$ and

$$\|K^{(p,p)}(\hat{\Sigma} \otimes \hat{\Sigma} - \Sigma^* \otimes \Sigma^*)\|_2 = \|(\hat{\Sigma} \otimes \hat{\Sigma} - \Sigma^* \otimes \Sigma^*)K^{(p,p)}\|_2 = \|\hat{\Sigma} \otimes \hat{\Sigma} - \Sigma^* \otimes \Sigma^*\|_2.$$

We obtain that

$$\begin{aligned}
\|\Gamma_2(\hat{\Sigma}) - \Gamma_2(\Sigma^*)\|_2 &\leq 2\|\hat{\Sigma} \otimes \hat{\Sigma} - \Sigma^* \otimes \Sigma^*\|_2 \\
&= 2\|\Delta_\Sigma \otimes \Delta_\Sigma + \Delta_\Sigma \otimes \Sigma^* + \Sigma^* \otimes \Delta_\Sigma + \Sigma^* \otimes \Sigma^* - \Sigma^* \otimes \Sigma^*\|_2 \\
&\leq 2\|\Delta_\Sigma \otimes \Delta_\Sigma\|_2 + 2\|\Delta_\Sigma \otimes \Sigma^*\|_2 + 2\|\Sigma^* \otimes \Delta_\Sigma\|_2 \\
&\leq 2\|\Delta_\Sigma\|_2^2 + 4\|\Sigma^*\|_2\|\Delta_\Sigma\|_2. \qquad \square
\end{aligned}$$

For a matrix $A \in \mathbb{R}^{p \times d}$, it holds that $\|A\|_\infty \leq \sqrt{d}\|A\|_2$. Then it follows from Lemma 4.1 and Lemma 4.2 that

$$\|(\Delta_\Gamma)._S\|_\infty \leq \sqrt{d}\left(4\|\Delta_\Sigma\|_2^2 + 8c_{\Sigma^*}\|\Delta_\Sigma\|_2\right). \tag{11}$$

We note that bounding $\|(\Delta_\Gamma)._S\|_\infty$ using $\|(\Delta_\Gamma)._S\|_\infty$, as was done in Lin et al. (2016), leads to a worse bound. While such an approach might seem simpler, it does not exploit the structure of the Hessian Γ in Lemma 2.2.

We now provide a bound on $\|\Delta_g\|_\infty$.

Lemma 4.3. *We have $\|\Delta_g\|_\infty \leq 2c_C\|\Delta_\Sigma\|_2$, where $c_C = \|vec(C)\|_2$.*

Proof. Similar to the proof of Lemma 4.1 and Lemma 4.2, we have

$$\begin{aligned}
\|\Delta_g\|_\infty &\leq \|\Delta_g\|_2 \\
&\leq c_C\|\Sigma^* \otimes I_p - (I_p \otimes \Sigma^*)K^{(p,p)} - \hat{\Sigma} \otimes I_p + (I_p \otimes \hat{\Sigma})K^{(p,p)}\|_2 \\
&\leq c_C(\|I_p \otimes (\hat{\Sigma} - \Sigma^*)\|_2 + \|(\hat{\Sigma} - \Sigma^*) \otimes I_p\|_2) \qquad \text{(since } \|K^{(p,p)}\|_2 = 1) \\
&= 2c_C\|\Delta_\Sigma\|_2. \qquad \square
\end{aligned}$$

The bounds in (11) and Lemma 4.3 depend on the spectral norm of Δ_Σ. We upper bound $\|\Delta_\Sigma\|_2$ under the assumption that $(x_i)_{i=1}^n$ are sub-Gaussian.

Theorem 4.4 (Theorem 6.5 in Wainwright (2019))**.** *Suppose that $(X_i)_{i=1}^n$ are σ sub-Gaussian random variables. Then the sample covariance matrix $\hat{\Sigma}$ in (3) satisfies*

$$\mathbb{P}\left(\frac{\|\hat{\Sigma} - \Sigma^*\|_2}{\sigma^2} \geq c_1\left\{\sqrt{\frac{p}{n}} + \frac{p}{n}\right\} + \delta\right) \leq c_2\exp(-c_3 n\min\{\delta, \delta^2\}) \quad \text{for all } \delta \geq 0,$$

where $\{c_j\}_{j=0}^3$ are universal constants.

The following form of the result will be convenient for us.

Corollary 4.5. *Let $\{c_j\}_{j=1}^3$ be the universal constants as in Theorem 4.4, where we take $c_1 > 1$. Suppose that $(X_i)_{i=1}^n$ are Gaussian random variables. For any $\epsilon \in (4c_1\sqrt{p/n}, 2)$, we have*

$$\mathbb{P}\left(\|\hat{\Sigma} - \Sigma^*\|_2 \geq \epsilon\right) \leq c_2 \exp\left(-\frac{c_3}{4}n\epsilon^2\right).$$

Proof. A Gaussian random vector is sub-Gaussian with parameter $\sigma = 1$. Set $\delta = \frac{\epsilon}{2}$. Since $\frac{p}{n} < \frac{\epsilon^2}{16c_1^2}$, we have

$$c_1\left\{\sqrt{\frac{p}{n}} + \frac{p}{n}\right\} + \delta < c_1\left\{\frac{\epsilon}{4c_1} + \frac{\epsilon^2}{16c_1^2}\right\} + \frac{\epsilon}{2} = \frac{\epsilon}{4} + \frac{\epsilon^2}{16c_1} + \frac{\epsilon}{2} < \frac{\epsilon}{4} + \frac{\epsilon}{4} + \frac{\epsilon}{2} = \epsilon.$$

Since $\delta < 1$, it holds that $\delta^2 < \delta$. Then

$$\mathbb{P}\left(\|\hat{\Sigma} - \Sigma^*\|_2 \geq \epsilon\right) \leq \mathbb{P}\left(\|\hat{\Sigma} - \Sigma^*\|_2 \geq c_1\left\{\sqrt{\frac{p}{n}} + \frac{p}{n}\right\} + \delta\right) \leq c_2 \exp(-c_3 n\delta^2)$$

$$= c_2 \exp\left(-\frac{c_3}{4}n\epsilon^2\right). \qquad \square$$

We finally have the following result.

Lemma 4.6. *In the event that*

$$\|\Delta_\Sigma\|_2 = \|\hat{\Sigma} - \Sigma^*\|_2 < \min\left\{\frac{\epsilon_1}{\sqrt{d}(4 + 8c_{\Sigma^*})}, \frac{\epsilon_2}{2c_C}\right\}$$

it holds that

$$\|(\Delta_\Gamma)_{\cdot S}\|_\infty < \epsilon_1 \quad and \quad \|\Delta_g\|_\infty < \epsilon_2.$$

Proof. The result follows directly from (11), where $\|\Delta_\Sigma\|_2^2 \leq \|\Delta_\Sigma\|_2$, and Lemma 4.3. $\qquad \square$

With this preparation we can complete the proof of our main result.

Proof of Corollary 3.2. Let $\epsilon = \sqrt{\tilde{c}d(\log p^{\tau_1})/n}$. Under the assumption on the sample size, we have $\epsilon \in (4c_1\sqrt{p/n}, 2)$. Corollary 4.5 then gives us that

$$\|\Delta_\Sigma\|_2 < \min\left\{\frac{\epsilon}{\sqrt{d}(4 + 8c_{\Sigma^*})}, \frac{\epsilon}{2c_C}\right\}$$

with probability at least $1 - c_2 p^{-\tau_1}$. Then $\|(\Delta_\Gamma)_{\cdot S}\|_\infty < \epsilon$ and $\|\Delta_g\|_\infty < \epsilon$, using Lemma 4.6. Furthermore, under the assumption on the sample size, we have $\epsilon \leq \frac{\alpha}{6c_{\Gamma^*}}$. The result follows from Theorem 3.1. $\qquad \square$

5. Irrepresentability Condition

The irrepresentability condition is vital for Theorem 3.1. The condition is well-known from the standard lasso regression, but appears to be much more subtle in the Lyapunov model. In regression and in the Lyapunov model, the irrepresentability condition makes an assumption about the Gram matrix in light of the signed support of the signal. However, the Gram matrix in regression depends solely on the predictors, whereas the Gram matrix for the Lyapunov model is obtained from the matrix $A(\Sigma)$ which depends on the signal itself; recall Example 2.1. In this section, we show that for every support corresponding to a directed acyclic graph (DAG), there
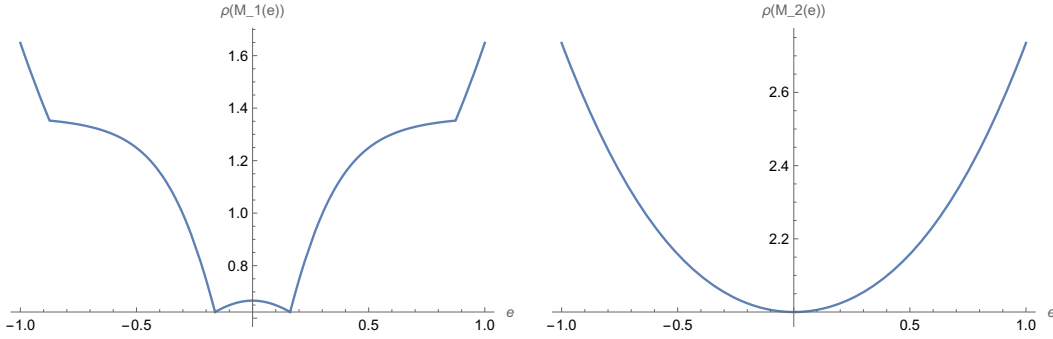
Fig 4: Values of the irrepresentability constants $\rho(M_1(e))$ and $\rho(M_2(e))$ for the two matrices from Example 1.1 plotted against the size of the off-diagonal entries e. Left: $\rho(M_1(e))$ where $\text{diag}(M_1(e)) = (-1/2, -1, -3/2)$. Right: $\rho(M_2(e))$ where $\text{diag}(M_2(e)) = (-3/2, -1, -1/2)$.

exists a drift matrix that fulfills the irrepresentability condition from Theorem 3.1. Our construction for DAGs is based on weak dependence among the variables and we also show that this same construction fails when the graph contains directed cycles. Indeed, further computational studies suggest that irrepresentability is difficult to satisfy when the graph is not acyclic.

In our study of the irrepresentability condition, we will consider the case where the volatility matrix C is a multiple of the identity, specifically, we assume $C = 2I_p$ *throughout this section.* (Other diagonal matrices C would also be tractable for analysis and would yield analogous conclusions.) Before proceeding, we recall that a matrix $M^* \in \text{Stab}_p$ with support S satisfies the irrepresentability condition if

$$\rho(M^*) := \|\Gamma^*_{S^c S}(\Gamma^*_{SS})^{-1}\text{sign}(\text{vec}(M^*)_S)\|_\infty \qquad (12)$$

is strictly smaller than 1; the condition in (10) stated an explicit gap $\alpha > 0$. In the sequel, we will refer to the number $\rho(M^*)$ as the *irrepresentability constant* of M^*.

5.1. Theoretical Analysis of the Irrepresentability Condition

In standard lasso regression, the irrepresentability condition is fulfilled when each irrelevant predictor exhibits little correlation with the active predictors. In particular, the condition would hold in a neighborhood of a diagonal Gram matrix. Under the Lyapunov model, it is not obvious how to suggest points for which the irrepresentability condition may be fulfilled. By the analogy with regression, natural candidates are obtained from drift matrices that are close to diagonal, for which the resulting covariance matrices are close to diagonal as well. Such candidates are the topic of the analysis presented in this subsection.

Example 5.1. Consider the graph $G = (V, E)$ from Example 1.1, a path on 3 nodes. For small $e \in \mathbb{R}$, we define two stable matrices $M_1(e)$ and $M_2(e)$ with support given by G. We set their diagonals to $\text{diag}(M_1(e)) = (-3/2, -1, -1/2)$ and $\text{diag}(M_2(e)) = (-1/2, -1, -3/2)$, respectively, and we set all non-zero off-diagonal entries equal to e. Note that the diagonal of $M_2(e)$ is the reverse of the diagonal of $M_1(e)$. In Figure 4, we plot the two irrepresentability constants $\rho(M_1(e))$ and $\rho(M_2(e))$ as functions of the off-diagonal value e. We observe that irrepresentability holds in a neighborhood of $M_1(0)$, but not around $M_2(0)$.

In the example just presented the order of diagonal entries is seen to impact whether irrepresentability holds near a diagonal matrix. As we prove in the theorem below this fact is not a coincidence but rather a general phenomenon.

Let $S \subseteq \{(i,j) : 1 \le i, j \le p\}$ be a given support set. We say that the irrepresentability condition for support S holds uniformly over a set $U \subset \mathrm{Stab}_p$ if there exists $\alpha > 0$ such that $\rho(M^*) \le 1 - \alpha$ for all $M^* \in U$ with support $S(M^*) = S$. By our convention, the edge set of a directed graph $G = (V, E)$ determines the support set $S_G = \{(j,i) : i \to j \in E\}$.

Theorem 5.2. *Let $G = (V, E)$ be a graph with p nodes. Let $M^0 = diag(-d_1, \ldots, -d_p)$ be a stable diagonal matrix. Then the irrepresentability condition for support S_G holds uniformly over a neighborhood of M^0 if and only if*

$$d_i < d_j \quad \text{for every edge} \quad j \to i \in E.$$

In particular, it is necessary that the graph G is a DAG.

Proof. Let $\Sigma^0 = \Sigma(M^0, C)$ be the covariance matrix associated to the drift matrix M^0. As we are assuming that $C = 2I_p$, we have

$$\Sigma^0 = -(M^0)^{-1} = \mathrm{diag}(1/d_1, \ldots, 1/d_p).$$

Writing $\Gamma^0 = \Gamma(\Sigma^0)$ for the resulting Gram matrix, we define the *local* irrepresentability constant

$$\tilde{\rho}_G(M^0) = \|\Gamma^0_{S_G^c S_G}(\Gamma^0_{S_G S_G})^{-1}\|_\infty.$$

If a small open ball around M^0 contains a matrix M, then the ball also contains all matrices that are obtained from M by negating one or more of the off-diagonal entries. Hence, by continuity, the irrepresentability condition for support S_G holds uniformly over a neighborhood of M^0 if and only if (i) the submatrix $\Gamma^0_{S_G S_G} = (\Gamma^0)_{S_G S_G}$ is invertible and (ii) $\tilde{\rho}_G(M^0) < 1$.

Since Σ^0 is diagonal, plugging it into the coefficient matrix from (6) gives a symmetric matrix with entries

$$A(\Sigma^0)_{(i,j),(k,l)} = \begin{cases} 2/d_k & \text{if } i = j = k = l, \\ 1/d_k & \text{if } i = k, \, j = l \text{ and } k \ne l, \\ 1/d_k & \text{if } i = l, \, j = k \text{ and } k \ne l, \\ 0 & \text{otherwise.} \end{cases}$$

The entries of the Gram matrix $\Gamma^0 = \Gamma(\Sigma^0)$ are the inner products of the columns of $A(\Sigma^0)$. That is,

$$\Gamma^0_{(i,j),(k,l)} = \begin{cases} 4/d_k^2 & \text{if } i = j = k = l, \\ 2/d_k^2 & \text{if } i = k, \, j = l \text{ and } k \ne l, \\ 2/(d_k d_l) & \text{if } i = l, \, j = k \text{ and } k \ne l, \\ 0 & \text{otherwise.} \end{cases}$$

Note that the only off-diagonal entries in Γ^0 occur when the row index is (i,j) and the column index is (j,i) with $i \ne j$. We display the matrices $A(\Sigma^0)$ and Γ^0 for a graph with $p = 3$ nodes in Example 5.3.

Case I: Graph contains a two-cycle. Suppose G contains a two-cycle, say $k \to l \to k$ with $k \ne l$. The two edges on the cycle index two columns of $A(\Sigma^0)$ that are linearly dependent. Indeed, the column indexed by (k,l) has only two nonzero entries in rows (k,l) and (l,k), both

of which are equal to d_k, and the same holds for the column indexed (l,k) except that the common value of its two nonzero entries is d_l. The columns (k,l) and (l,k) of Γ^0 are similarly linearly dependent. Hence, the submatrix $\Gamma^0_{S_G S_G}$ fails to be invertible, if the graph G contains a two-cycle. Consequently, the irrepresentability condition holds uniformly over a neighborhood of M^0 only if G is free of two-cycles, in which case we call G *simple*.

Case II. Graph is simple. In the rest of the proof suppose that G is simple. In this case, the submatrix $\Gamma^0_{S_G S_G}$ is diagonal with entries

$$\Gamma^0_{(k,l),(k,l)} = \begin{cases} 4/d_k^2 & \text{if } k = l, \\ 2/d_k^2 & \text{if } k \neq l, \end{cases}$$

where $l \to k$ is an edge of G. The second submatrix of interest, $\Gamma^0_{S_G^c S_G}$, also has only one nonzero entry in each column. If $l \to k$ is an edge, indexing column (k,l), then the entry is

$$(\Gamma^0_{S_G^c S_G})_{(l,k),(k,l)} = 2/(d_k d_l).$$

Note that G being simple implies that $k \to l$ is not an edge of G. Multiplying the second submatrix to the inverse of the first, we obtain that

$$(\Gamma^0_{S_G^c S_G}(\Gamma^0_{S_G S_G})^{-1})_{(i,j),(k,l)} = \begin{cases} d_k/d_l & \text{if } (i,j) = (l,k) \text{ and } (k,l) \in S_G, (l,k) \in S_G^c, \\ 0 & \text{otherwise.} \end{cases}$$

Since $\tilde{\rho}_G(M^0)$ is obtained via the maximum absolute row sum, we have $\tilde{\rho}_G(M^0) < 1$ if and only if $d_i/d_j < 1$ for all pairs $(i,j) \in S_G$, or equivalently, all edges $j \to i \in E$, as the theorem claims. $\qquad\square$

We illustrate the matrix calculations in the proof of Theorem 5.2 for a graph on $p = 3$ nodes.

Example 5.3. We consider the 3-chain $G = (V, E)$ displayed in Figure 1, and the matrices

$$M^0 = \text{diag}(-d_1, -d_2, -d_3) \quad \text{and} \quad \Sigma^0 = \text{diag}(1/d_1, 1/d_2, 1/d_3).$$

Ordering rows and columns as $(1,1), (1,2), (1,3), (2,1), (2,2), (2,3), (3,1), (3,2), (3,3)$, we find

$$A(\Sigma^0) = \begin{pmatrix}
2/d_1 & 0 & 0 & 0 & 0 & 0 & 0 & 0 & 0 \\
0 & 1/d_1 & 0 & 1/d_2 & 0 & 0 & 0 & 0 & 0 \\
0 & 0 & 1/d_1 & 0 & 0 & 0 & 1/d_3 & 0 & 0 \\
0 & 1/d_1 & 0 & 1/d_2 & 0 & 0 & 0 & 0 & 0 \\
0 & 0 & 0 & 0 & 2/d_2 & 0 & 0 & 0 & 0 \\
0 & 0 & 0 & 0 & 0 & 1/d_2 & 0 & 1/d_3 & 0 \\
0 & 0 & 1/d_1 & 0 & 0 & 0 & 1/d_3 & 0 & 0 \\
0 & 0 & 0 & 0 & 0 & 1/d_2 & 0 & 1/d_3 & 0 \\
0 & 0 & 0 & 0 & 0 & 0 & 0 & 0 & 2/d_3
\end{pmatrix}$$

and

$$\Gamma^0 = \begin{pmatrix}
4/d_1^2 & 0 & 0 & 0 & 0 & 0 & 0 & 0 & 0 \\
0 & 2/d_1^2 & 0 & 2/d_1 d_2 & 0 & 0 & 0 & 0 & 0 \\
0 & 0 & 2/d_1^2 & 0 & 0 & 0 & 2/d_1 d_3 & 0 & 0 \\
0 & 2/d_1 d_2 & 0 & 2/d_2^2 & 0 & 0 & 0 & 0 & 0 \\
0 & 0 & 0 & 0 & 4/d_2^2 & 0 & 0 & 0 & 0 \\
0 & 0 & 0 & 0 & 0 & 2/d_2^2 & 0 & 2/d_2 d_3 & 0 \\
0 & 0 & 2/d_1 d_3 & 0 & 0 & 0 & 2/d_3^2 & 0 & 0 \\
0 & 0 & 0 & 0 & 0 & 2/d_2 d_3 & 0 & 2/d_3^2 & 0 \\
0 & 0 & 0 & 0 & 0 & 0 & 0 & 0 & 4/d_3^2
\end{pmatrix}.$$

Since $S_G = \{(1,1),(2,1),(2,2),(3,2),(3,3)\}$ and $S_G^c = \{(1,2),(1,3),(3,1),(2,3)\}$, we obtain

$$(\Gamma^0_{S_G S_G})^{-1} = \text{diag}(d_1^2/4, d_2^2/2, d_2^2/4, d_3^2/2, d_3^2/4),$$

$$\Gamma^0_{S_G^c S_G} = \begin{pmatrix} 0 & 2/d_1 d_2 & 0 & 0 & 0 \\ 0 & 0 & 0 & 0 & 0 \\ 0 & 0 & 0 & 0 & 0 \\ 0 & 0 & 0 & 2/d_2 d_3 & 0 \end{pmatrix},$$

and

$$\Gamma^0_{S_G^c S_G}(\Gamma^0_{S_G S_G})^{-1} = \begin{pmatrix} 0 & 0 & 0 & 0 & 0 \\ 0 & d_2/d_1 & 0 & 0 & 0 \\ 0 & 0 & 0 & 0 & 0 \\ 0 & 0 & 0 & d_3/d_2 & 0 \end{pmatrix}.$$

To have $\|\Gamma^0_{S_G^c S_G}(\Gamma^0_{S_G S_G})^{-1}\|_\infty < 1$, we need $d_2/d_1 < 1$ and $d_3/d_2 < 1$. With the edges $1 \to 2$ and $2 \to 3$ present in G, this requirement coincides with the statement of Theorem 5.2.

5.2. Simulation Studies

We have shown that for every DAG there exist non-trivial stable signals such that the irrepresentability condition holds. These signals were constructed to be in a neighborhood of diagonal matrices whose diagonal entries are ordered in accordance with the topological ordering of the DAG. As the size of the graphs increases, this diagonal ordering becomes more restrictive. Moreover, there might be signals that have a different diagonal ordering, but still fulfill the irrepresentability condition. In order to investigate these points, we simulate stable signals according to a uniform distribution and study how often the condition is fulfilled. Our simulations also consider simple and non-simple cyclic graphs, for which we do not know how to give a general construction of signals that satisfy irrepresentability.

Given a graph $G = (V, E)$, we generate signals $M^* \in \text{Stab}_p(E)$ by drawing from the uniform distribution on the subset of matrices in $\text{Stab}_p(E)$ that have all entries in $[-1, 1]$. The sampling is carried out by rejection sampling, with rejection of matrices that are not stable.

We consider connected graphs with $p = 2, 3, 4$ nodes and at most $p(p + 1)/2$ edges. This includes all DAGs but also many cyclic graphs. Furthermore, we only consider one labeling of vertices for every graph. For every graph, we check for one million simulated signals M^* if $\rho(M^*) < 1$ and store the signals that meet the irrepresentability condition (10). The frequency of signals that meet the irrepresentability condition is shown in Figure 5.

We observe the overall tendency that the higher the number of edges, the lower the percentage of signals that fulfill the irrepresentability condition. However, the decrease is not monotonic. This is explained in part by the fact that the number of ordering conditions on the diagonal elements in Theorem 5.2 increases only if an additional edge refines the ordering of nodes.

Example 5.4. Consider the graph shown in Figure 6, which has the highest frequency of irrepresentability among the graphs with three edges. Since there is no edge between the nodes $\{1, 2, 3\}$, the only conditions on the diagonal are $d_4/d_1 < 1, d_4/d_2 < 1$ and $d_4/d_3 < 1$.

Remark 5.5. While the ordering of diagonal entries plays an important role, our simulations also identified many examples in which irrepresentability is satisfied but the ordering condition on the diagonal from Theorem 5.2 does not hold.
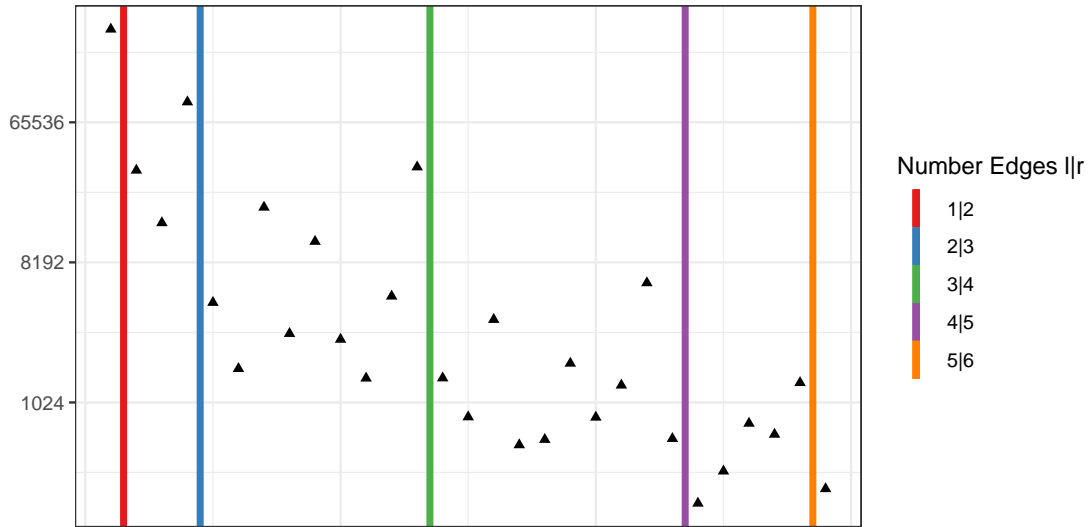
Fig 5: Frequency of the irrepresentability condition being met for one million simulated stable matrices M^* for DAGs up to 4 nodes. The number of edges is given by the coloring.
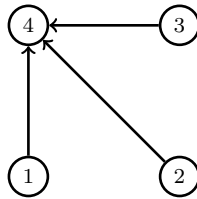

Fig 6: The graph on three nodes with highest frequency of simulated signals satisfying irrepresentability.

Corollary 3.2 together with an argument similar to that in Zhao and Yu (2006) shows that the irrepresentability condition is almost necessary. It is natural to expect worse results in terms of support recovery for signals that do not satisfy the irrepresentability condition than for those that do. Through a simulation, we illustrate the difference in support recovery. For every DAG, we select 100 signals that satisfy the irrepresentability condition and compare them with 100 randomly selected signals (as earlier from a uniform distribution of stable matrices with entries between -1 and 1). We then sample data sets of size $n = 100$ from the normal distribution given by these signals, and use the Direct Lyapunov Lasso to recover the support along a regularization path. We use the area under the curve (AUC) as a measure of support recovery. Figure 7 illustrates the results averaged over the 100 independent signals.

We observe that the signals that satisfy the irrepresentability condition score better than the randomly selected ones. The difference in support recovery increases with the number of edges, which may be explained by the fact that randomly selected signals are less likely to satisfy the irrepresentability condition as the number of edges increases—as illustrated in Figure 5.

Finally, we report on how often the irrepresentability condition is satisfied with graphs that have cycles. We first single out graphs that are not simple, i.e., have at least one two-cycle. Following the simulation setup leading to Figure 5, we investigate how often the irrepresentability condition is satisfied for non-simple graphs without cycles of length ≥ 3, out of 10,0000 randomly
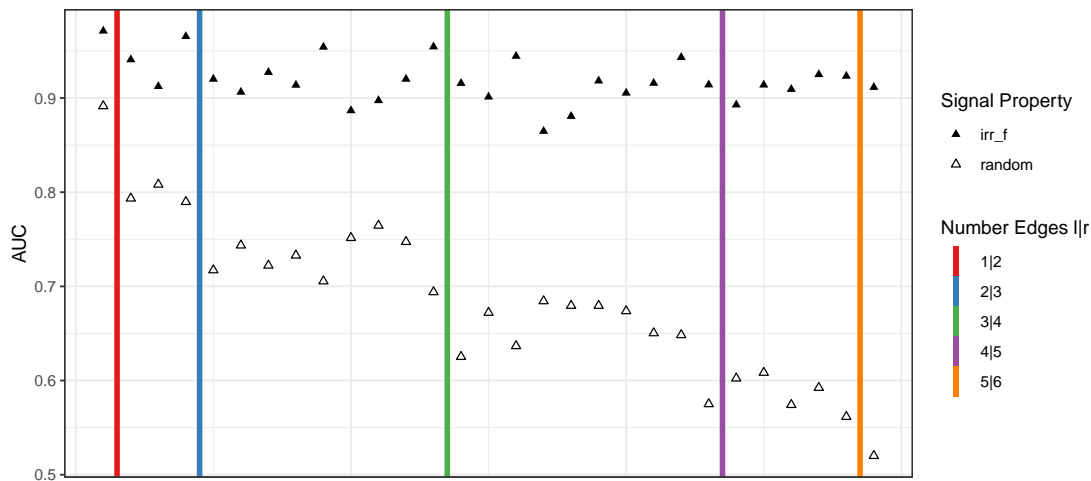
Fig 7: The AUC values for DAGs with up to 4 nodes. The number of edges is given by the coloring. **Empty:** irrepresentability condition in general not fulfilled, **Full:** irrepresentability condition fulfilled.

drawn stable signals. We only consider non-simple graphs for which almost all parameters can be uniquely recovered from the joint distribution of observed variables. Compared to the DAGs with a similar number of edges (and including a scaling factor 100 for the smaller number of random draws), we observe that non-simple graphs (free of three-cycles) satisfy the irrepresentability condition with a similar frequency.

For simple graphs with cycles, it is surprisingly difficult to find parameters for which the irrepresentability condition holds. Extensive computation was necessary to present one example for every simple cyclic graph up to four nodes. One such signal for each graph is shown in Table 1 in Appendix B. We were not able to discern structure that would suggest how to construct such examples in general.

6. Conclusion

We investigated model selection properties of the Direct Lyapunov Lasso when applied to data distributed according to the graphical continuous Lyapunov model. Although the optimization problem that Direct Lyapunov Lasso solves is similar to the lasso penalized linear regression objective, there are several surprising differences. The role of the matrix $A(\Sigma)$, which is analogous to the design matrix in the regression setting, is subtle under the Lyapunov model. We established a reasonable bound on sample complexity by careful investigation of the Hessian matrix whose elements are sums of p products of covariances. Furthermore, while the irrepresentable condition can be assumed in the linear regression setting, this is not the case for the model considered here. Indeed, our detailed analysis of the irrepresentability condition illustrates the reasons for its restrictiveness. We formulated conditions under which the irrepresentability condition is guaranteed to hold for DAGs based on the topological ordering of the nodes and provided insight into why a similar result is difficult to obtain in the presence of cyclic structures. Simulations further provided evidence to the extent to which one can hope that the irrepresentability condition is satisfied for a randomly drawn signals. From the simulation we also observe that many true signals for DAGs, which meet the irrepresentability condition, have a diagonal that does not follow the topological ordering of the nodes. As a result, ordering the diagonal is not
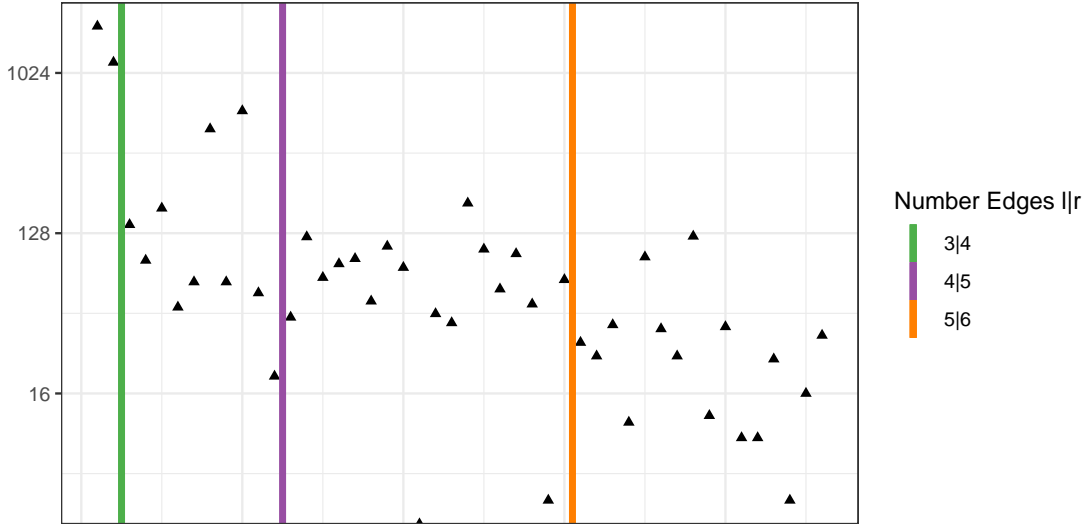
Fig 8: Frequency of the irrepresentability condition being met for 100,000 simulated stable matrices M^* for non-simple graphs without cycles of length ≥ 3, up to 4 nodes, and up to 6 edges. The number of edges is given by the coloring.

a necessary condition. Even in the finite sample setting, the irrepresentability condition being met proves to have a measurable positive impact on support recovery. For simple cyclic graphs, the irrepresentability condition is rarely satisfied. The Direct Lyapunov Lasso (Fitch, 2019) is a powerful and easy-to-implement tool for model selection of graphs from cross-sectional data in finite sample settings where the irrepresentability condition holds. Simulations show that this condition is rarely met in practice, but is needed for support recovery.

Acknowledgements

Appendix A: Proofs for Section 3

A.1. Proof of Theorem 3.1

We use the PDW technique to prove the result. The estimate $\hat{M}$ satisfies the KKT conditions

$$\hat{\Gamma}\text{vec}(\hat{M}) - \hat{g} + \lambda\hat{z} = 0, \tag{13}$$

where $\hat{z} \in \partial\|\text{vec}(\hat{M})\|_1$ is an element of the subdifferential of the ℓ_1-norm, that is, the elements of the vector $\hat{z} \in \mathbb{R}^{p^2}$ satisfy that elements

$$\hat{z}_{(i,j)} = \begin{cases} \text{sign}(\text{vec}(\hat{M})_{(i,j)}) & \text{if } \text{vec}(\hat{M})_{(i,j)} \neq 0, \\ \in [-1,1] & \text{if } \text{vec}(\hat{M})_{(i,j)} = 0. \end{cases}$$

Here, we index $\hat{z}$ by pairs (i, j) with $1 \leq i, j \leq p$. The optimization problem in (9) is convex as Γ is positive semidefinite by construction, and the KKT conditions are necessary and sufficient for a solution to be optimal for the problem. The PDW technique constructs, in three steps, a primal-dual pair $(\hat{M}, \hat{z})$ that satisfies (13) and has the support of $\hat{M}$ contained in S.

Since the true signal $M^* \in \text{Stab}_p$ and $C \in PD_p$, there exists a unique positive definite Σ^* determined by the continuous Lyapunov equation in (2). As a result

$$\Gamma^* \text{vec}(M^*) - g^* = 0,$$

and we can rewrite the KKT conditions in (13) in the following block form

$$\begin{bmatrix} \Gamma^*_{SS} & \Gamma^*_{SS^c} \\ \Gamma^*_{S^cS} & \Gamma^*_{S^cS^c} \end{bmatrix} \begin{bmatrix} (\Delta_M)_S \\ (\Delta_M)_{S^c} \end{bmatrix} + \begin{bmatrix} (\Delta_\Gamma)_{SS} & (\Delta_\Gamma)_{SS^c} \\ (\Delta_\Gamma)_{S^cS} & (\Delta_\Gamma)_{S^cS^c} \end{bmatrix} \begin{bmatrix} \text{vec}(\hat{M})_S \\ \text{vec}(\hat{M})_{S^c} \end{bmatrix} + \begin{bmatrix} (\Delta_g)_S \\ (\Delta_g)_{S^c} \end{bmatrix} + \lambda \begin{bmatrix} \hat{z}_S \\ \hat{z}_{S^c} \end{bmatrix} = \begin{bmatrix} 0 \\ 0 \end{bmatrix},$$

where $\Delta_M = \text{vec}(\hat{M}) - \text{vec}(M^*)$. We now construct a pair $(\hat{M}, \hat{z})$ that satisfies the equation.

Step 1. We solve the restricted optimization problem

$$\text{vec}(\tilde{M}) = \arg \min_{\text{vec}(M)_{S^c} = 0} \frac{1}{2} \text{vec}(M)^\top \hat{\Gamma} \text{vec}(M) - \hat{g}^\top \text{vec}(M) + \lambda \|\text{vec}(M)\|_1. \tag{14}$$

Since Γ^*_{SS} is invertible, we can follow the derivation in equation (7.8) of Lin et al. (2016) to show that, under our assumptions, $\hat{\Gamma}_{SS}$ is also invertible. Therefore, the solution $\text{vec}(\tilde{M})$ is unique. Furthermore, we have

$$(\text{vec}(\tilde{M}))_S = (\hat{\Gamma}_{SS})^{-1}(\hat{g}_S - \lambda \text{sign}((\text{vec}(\tilde{M}))_S)).$$

Let $\tilde{\Delta}_M = \text{vec}(\tilde{M}) - \text{vec}(M^*)$. Following the proof of Theorem 1 in Lin et al. (2016), we have

$$\|\tilde{\Delta}_M\|_\infty \leq \frac{c_{\Gamma^*}}{1 - \alpha/6} \cdot \frac{6 - \alpha}{3(2 - \alpha)} \lambda = \frac{2c_{\Gamma^*}}{2 - \alpha}.$$

Step 2. Let $\tilde{z}_S = \text{sign}(\text{vec}(\tilde{M})_S)$. Then $\tilde{z}_S \in \partial \|\text{vec}(\tilde{M})\|_1$.

Step 3. Let

$$\tilde{z}_{S^c} = \frac{1}{\lambda} \Big[-\Gamma^*_{S^cS}(\Gamma^*_{SS})^{-1}((\Delta_\Gamma)_{SS} \text{vec}(\tilde{M})_S + (\Delta_g)_S) + (\Delta_\Gamma)_{S^cS} \text{vec}(\tilde{M})_S$$
$$+ (\Delta_g)_{S^c} + \lambda \Gamma^*_{S^cS}(\Gamma^*_{SS})^{-1} \text{sign}(\text{vec}(\tilde{M})_S) \Big]. \tag{15}$$

We show that $\|\tilde{z}_{S^c}\|_1 < 1$, which is a dual feasibility condition. Once this is shown, we have that the pair $(\text{vec}(\hat{M}), \tilde{z})$ satisfies (13) by construction, and $(\text{vec}(\hat{M}), \hat{z}) = (\text{vec}(\tilde{M}), \tilde{z})$ is the solution to the optimization problem in (9). Furthermore, Lemma 1 of Wainwright (2009) implies that the strict dual feasibility implies that $\hat{S} \subseteq S$. Following Theorem 1 in Lin et al. (2016), we have

$$\|\tilde{z}_{S^c}\|_\infty \leq \underbrace{\frac{2 - \alpha}{\lambda} \|(\Delta_\Gamma)._S \text{vec}(M^*)_S\|_\infty}_{G_1} + \underbrace{\frac{2 - \alpha}{\lambda} \|(\Delta_\Gamma)._S\|_\infty \|\Delta_S\|_\infty}_{G_2} + \underbrace{\frac{2 - \alpha}{\lambda} \|\Delta_g\|_\infty}_{G_3} + (1 - \alpha).$$

For G_1, we have that

$$G_1 \leq \frac{2 - \alpha}{\lambda} \|(\Delta_\Gamma)._S\|_\infty \|\text{vec}(M^*)\|_\infty = \frac{2 - \alpha}{\lambda} c_{M^*} \epsilon_1 \leq \frac{\alpha}{3}.$$

For G_3, we have that

$$G_3 = \frac{2-\alpha}{\lambda}\|\Delta_g\|_\infty < \frac{2-\alpha}{\lambda}\epsilon_2 \leq \frac{\alpha}{3}.$$

Finally, for G_2, we have that

$$G_2 < \frac{2-\alpha}{\lambda} \cdot \frac{\alpha}{6c_{\Gamma^*}} \cdot \epsilon_1 \cdot \frac{c_{\Gamma^*}}{1-\alpha/6} \cdot \frac{6-\alpha}{3(2-\alpha)} < \frac{\alpha}{3}.$$

Combining these bounds, we have that $\|\tilde{z}_{S^c}\|_\infty < 1$, which establishes the strict dual feasibility.
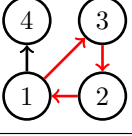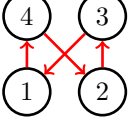
Finally, for any $(j,k) \in S$, we have that
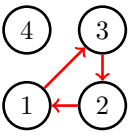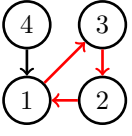
$$|\hat{M}_{jk}| \geq |M^*_{jk}| - |\hat{M}_{jk} - M^*_{jk}| > \min_{\substack{1 \leq j < k \leq p \\ (j,k) \in S}} |M^*_{jk}| - \|\mathrm{vec}(\hat{M}) - \mathrm{vec}(M^*)\|_\infty > 0,$$

which shows that $\hat{S} = S$.

Appendix B: Cyclic Graphs fulfilling Irrepresentability

In Table 1, we list cyclic graphs on 4 nodes together with examples of drift matrices M that satisfy the irrepresentability condition. The selection of graphs includes all graphs that contain at least one directed cycle and are simple (i.e., do not contain a two-cycle).

Table 1: Left: All simple cyclic graphs with 4 nodes, up to relabelling of the nodes. Edges on cycles are highlighted in red. **Right:** Specific choice of matrices M matching the graph on the left and fulfilling irrepresentability, all entries are rounded to 10 digits.

$$\begin{pmatrix} -0.0444620792 & -0.5733500496 & 0.0000000000 & 0.0000000000 \\ 0.0000000000 & -0.0153532191 & 0.0054622865 & 0.0000000000 \\ 0.8317033453 & 0.0000000000 & -0.8824298000 & 0.0000000000 \\ 0.0000000000 & 0.0000000000 & 0.0000000000 & -0.3405775614 \end{pmatrix}$$

$$\begin{pmatrix} -0.9780979650 & 0.1042322782 & 0.0000000000 & 0.3752107187 \\ 0.0000000000 & -0.7998522464 & -0.4260628200 & 0.0000000000 \\ 0.2079165080 & 0.0000000000 & -0.6517819995 & 0.0000000000 \\ 0.0000000000 & 0.0000000000 & 0.0000000000 & -0.8112314143 \end{pmatrix}$$

$$\begin{pmatrix} -0.6792729949 & -0.6022921619 & 0.0000000000 & 0.0000000000 \\ 0.0000000000 & -0.1733464822 & 0.5762203289 & 0.0000000000 \\ 0.0383909321 & 0.0000000000 & -0.1785332798 & 0.0000000000 \\ 0.2089620568 & 0.0000000000 & 0.0000000000 & -0.6556593408 \end{pmatrix}$$

$$\begin{pmatrix} -0.5008390141 & 0.0000000000 & -0.3301411900 & 0.0000000000 \\ 0.0000000000 & -0.0754047022 & 0.0000000000 & -0.2224099669 \\ 0.0000000000 & 0.9894780936 & -0.8953534714 & 0.0000000000 \\ -0.4568265276 & 0.0000000000 & 0.0000000000 & -0.6545859827 \end{pmatrix}$$

$$\begin{pmatrix} -0.9852473154 & 0.0237436080 & 0.0000000000 & -0.1801203806 \\ 0.0000000000 & -0.9146776730 & -0.6301784553 & -0.3625553502 \\ 0.0314035588 & 0.0000000000 & -0.7371845325 & 0.0000000000 \\ 0.0000000000 & 0.0000000000 & 0.0000000000 & -0.2936787312 \end{pmatrix}$$

$$\begin{pmatrix} -0.6168078599 & -0.4643970933 & 0.0000000000 & 0.0000000000 \\ 0.0000000000 & -0.8265482867 & 0.0118716909 & 0.4726413568 \\ 0.3998511671 & 0.0000000000 & -0.8792877044 & 0.0000000000 \\ -0.5496377517 & 0.0000000000 & 0.0000000000 & -0.7865214688 \end{pmatrix}$$

$$\begin{pmatrix} -0.2066421132 & -0.0034684981 & 0.1383411973 & 0.0000000000 \\ 0.0000000000 & -0.9617960961 & 0.0000000000 & -0.7641737331 \\ 0.0000000000 & -0.3169060163 & -0.7561623598 & 0.0000000000 \\ -0.7012514030 & 0.0000000000 & 0.0000000000 & -0.2419070452 \end{pmatrix}$$

$$\begin{pmatrix} -0.8234110032 & -0.6069790549 & 0.0000000000 & 0.0000000000 \\ 0.0000000000 & -0.4768311884 & 0.0000000000 & -0.5430481988 \\ -0.1151224086 & 0.5541216009 & -0.8947804412 & 0.0000000000 \\ -0.1818817416 & 0.0000000000 & 0.0000000000 & -0.6244826200 \end{pmatrix}$$

$$\begin{pmatrix} -0.7566250684 & 0.1517044385 & 0.0000000000 & 0.0068894741 \\ 0.0000000000 & -0.9917302341 & 0.5077337530 & 0.3153799707 \\ 0.0895817326 & 0.0000000000 & -0.7472212519 & -0.1730670566 \\ 0.0000000000 & 0.0000000000 & 0.0000000000 & -0.3600410065 \end{pmatrix}$$

$$\begin{pmatrix} -0.8680259003 & 0.4557597358 & -0.0925138230 & 0.0000000000 \\ 0.0000000000 & -0.9139470784 & -0.1607573517 & 0.3138186112 \\ 0.0000000000 & 0.0000000000 & -0.9212171654 & -0.9521876550 \\ -0.5101859323 & 0.0000000000 & 0.0000000000 & -0.2475099666 \end{pmatrix}$$

$$\begin{pmatrix} -0.6688544271 & 0.0000000000 & -0.7215559445 & 0.0000000000 \\ -0.4272868899 & -0.9967063963 & 0.0374428187 & -0.8531300114 \\ 0.0000000000 & 0.0000000000 & -0.6779836947 & -0.5781906121 \\ -0.6749138949 & 0.0000000000 & 0.0000000000 & -0.5980373188 \end{pmatrix}$$

References

Carlos Améndola, Philipp Dettling, Mathias Drton, Federica Onori, and Jun Wu. Structure learning for cyclic linear causal models. In *Proceedings of the 36th Conference on Uncertainty in Artificial Intelligence (UAI)*, pages 999–1008, 2020.

Dennis S. Bernstein. *Scalar, vector, and matrix mathematics.* Princeton University Press, Princeton, NJ, 2018.

Stephan Bongers and Joris M. Mooij. From random differential equations to structural causal models: the stochastic case. *arXiv.org preprint*, 1803.08784, 2018.

Stephan Bongers, Patrick Forré, Jonas Peters, and Joris M. Mooij. Foundations of structural causal models with cycles and latent variables. *Ann. Statist.*, 49(5):2885–2915, 2021.

Philipp Dettling, Roser Homs, Carlos Amendola, Mathias Drton, and Niels Richard Hansen. Identifiability in continuous Lyapunov models, 2022. Forthcoming.

Mathias Drton, Christopher Fox, and Y. Samuel Wang. Computation of maximum likelihood estimates in cyclic structural equation models. *Ann. Statist.*, 47(2):663–690, 2019.

Franklin M Fisher. A correspondence principle for simultaneous equation models. *Econometrica*, 38(1):73–92, 1970.

Katherine E. Fitch. Learning directed graphical models from Gaussian data. *CoRR*, abs/1906.08050, 2019.

Lina Lin, Mathias Drton, and Ali Shojaie. Estimation of high-dimensional graphical models using regularized score matching. *Electron. J. Stat.*, 10(1):806–854, 2016.

Marloes Maathuis, Mathias Drton, Steffen Lauritzen, and Martin Wainwright, editors. *Handbook of graphical models*. Chapman & Hall/CRC Handbooks of Modern Statistical Methods. CRC Press, Boca Raton, FL, 2019.

Søren Wengel Mogensen, Daniel Malinsky, and Niels Richard Hansen. Causal learning for partially observed stochastic dynamical systems. In *Proceedings of the 34th conference on Uncertainty in Artificial Intelligence (UAI)*, pages 350–360, 2018.

Joris M. Mooij, Dominik Janzing, and Bernhard Schölkopf. From ordinary differential equations to structural causal models: The deterministic case. In *Proceedings of the 29th Conference on Uncertainty in Artificial Intelligence (UAI)*, pages 440–448, 2013.

Judea Pearl. *Causality*. Cambridge University Press, Cambridge, second edition, 2009.

Jonas Peters, Dominik Janzing, and Bernhard Schölkopf. *Elements of causal inference*. Adaptive Computation and Machine Learning. MIT Press, Cambridge, MA, 2017.

Pradeep Ravikumar, Martin J. Wainwright, Garvesh Raskutti, and Bin Yu. High-dimensional covariance estimation by minimizing ℓ_1-penalized log-determinant divergence. *Electron. J. Stat.*, 5:935–980, 2011.

Thomas Richardson. A discovery algorithm for directed cyclic graphs. In *Uncertainty in Artificial Intelligence (Portland, OR, 1996)*, pages 454–461. Morgan Kaufmann, San Francisco, CA, 1996.

Peter Spirtes, Clark Glymour, and Richard Scheines. *Causation, prediction, and search*. Adaptive Computation and Machine Learning. MIT Press, Cambridge, MA, second edition, 2000.

Gherardo Varando and Niels Richard Hansen. Graphical continuous Lyapunov models. In *Proceedings of the 36th Conference on Uncertainty in Artificial Intelligence (UAI)*, pages 989–998, 2020.

Martin J. Wainwright. Sharp thresholds for high-dimensional and noisy sparsity recovery using ℓ_1-constrained quadratic programming (lasso). *IEEE Transactions on Information Theory*, 55(5):2183–2202, 2009.

Martin J. Wainwright. *High-dimensional statistics*, volume 48 of *Cambridge Series in Statistical and Probabilistic Mathematics*. Cambridge University Press, Cambridge, 2019.

Peng Zhao and Bin Yu. On model selection consistency of Lasso. *J. Mach. Learn. Res.*, 7: 2541–2563, 2006.